J Biol Inorg Chem
DOI 10.1007/s00775-014-1211-9

ORIGINAL PAPER

Interaction of the anticancer gallium(III) complexes of 8-hydroxyquinoline and maltol with human serum proteins

Éva A. Enyedy · Orsolya Dömötör · Krisztina Bali · Anasztázia Heténi · Tiziano Tuccinardi · Bernhard K. Keppler

Received: 19 May 2014 / Accepted: 27 October 2014

Abstract Tris(8-quinolinolato)gallium(III) (KP46) and tris(maltolato)gallium(III) (GaM) are promising orally active antitumor metallodrugs currently undergoing clinical trials. Their interaction with human serum albumin (HSA) and transferrin (Tf) was studied in detail in aqueous solution by the combination of various methods such as spectrofluorometry, UV–vis spectrophotometry, ^{1}H and saturation transfer difference NMR spectroscopy, and ultrafiltration–UV–vis spectrophotometry. Binding data were evaluated quantitatively. Tf was found to replace the original ligand much less efficiently in KP46 than in GaM, whereas a significant noncovalent binding of KP46 with HSA (log $K' = 4.04$) retaining the coordination environment around gallium(III) was found. The interaction between HSA and KP46 was also confirmed by protein–complex modeling calculations. On the basis of the conditional stability constants, the distribution of gallium(III) in serum was computed and compared for these metallodrugs under physiological conditions, and revealed the prominent role of HSA in the case of KP46 and that of Tf for GaM.

Keywords Solution equilibrium · Albumin · Transferrin · Binding affinity · Fluorescence

Abbreviations

apoTf	Apotransferrin
GaM	Tris(3-hydroxy-2-methyl-4*H*-pyran-4-onato) gallium(III)
HEPES	4-(2-Hydroxyethyl)-1-piperazineethanesulfonic acid
HMM	High molecular mass
HSA	Human serum albumin
HQ	8-Hydroxyquinoline
KP46	Tris(8-quinolinolato)gallium(III)
LMM	Low molecular mass
PDB	Protein Data Bank
STD	Saturation transfer difference
Tf	Human serum transferrin

Introduction

The field of the metal-based anticancer drugs began with cisplatin, one of the leading agents in clinical use [1]. Numerous Ga(III) complexes also inhibit tumor growth and gallium was the second metal ion, after platinum, to be administered to cancer patients [2–5]. Remarkably, the simple salt $Ga(NO_3)_3$ shows antineoplastic effects in particular for the treatment of lymphoma and bladder cancer and has a therapeutic effect in cancer-related hypercalcemia

Electronic supplementary material The online version of this article (doi:10.1007/s00775-014-1211-9) contains supplementary material, which is available to authorized users.

É. A. Enyedy (✉) · O. Dömötör · K. Bali
Department of Inorganic and Analytical Chemistry, University of Szeged, Dóm tér 7, Szeged 6720, Hungary
e-mail: enyedy@chem.u-szeged.hu

O. Dömötör
MTA-SZTE Bioinorganic Chemistry Research Group, Dóm tér 7, Szeged 6720, Hungary

A. Heténi
Department of Medical Chemistry, University of Szeged, Dóm tér 8, Szeged 6720, Hungary

T. Tuccinardi
Department of Pharmacy, University of Pisa, 56126 Pisa, Italy

B. K. Keppler
Institute of Inorganic Chemistry, University of Vienna, Waehringer Str. 42, 1090 Vienna, Austria

Published online: 15 November 2014

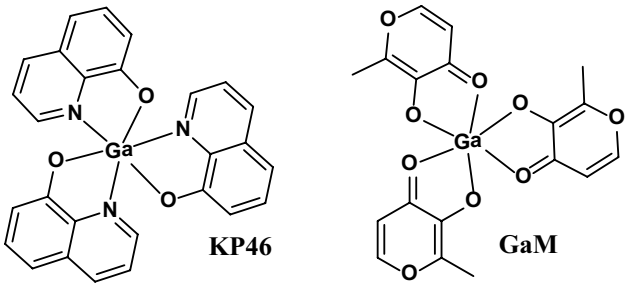

Structure 1 Structures of the Ga(III) complexes: tris(8-quinolinolato)gallium(III) (*KP46*) and tris(3-hydroxy-2-methyl-4*H*-pyran-4-onato)gallium(III) (*GaM*)

(Ganite™ in clinical use) [4]. As orally administered gallium salts are not sufficiently bioavailable, the therapeutic index can be improved efficiently by the application of charge-neutral complexes [5]. Two Ga(III) complexes have entered clinical trials so far as orally active metallodrugs: tris(3-hydroxy-2-methyl-4*H*-pyran-4-onato)gallium(III) (GaM) and tris(8-quinolinolato)gallium(III) (KP46) [2, 3] (see Structure 1). Orally administered KP46 was found to be well tolerated in a phase I dose-escalation study in patients with advanced malignant solid tumors and showed no renal toxicity [6]. GaM was also well tolerated in phase I clinical trials without dose-limiting toxicity [3]. The latest clinical phase I/II studies with GaM for the treatment of bladder cancer, lymphoma, multiple myeloma, and prostatic neoplasms were terminated in 2005; however, no results were published [7]. A recent case study pointed out the clinical benefit of GaM in the treatment of hepatocellular carcinoma [8].

The primary target of gallium compounds is supposed to be the iron-containing ribonucleotide reductase, the rate-determining enzyme in the supply of deoxyribonucleotides for DNA synthesis required for cell proliferation [9]. Ga(III) is able to bind to the iron sites of human serum transferrin (Tf), which promotes its cellular absorption [10], in particular in proliferating cancer cells with strong iron demand and overexpressed Tf receptors [9, 11]. On the other hand, interaction of Ga(III) with Tf might be modulated by the application of carrier ligands since competition can occur between the protein and the coordinating ligands, and this process strongly depends on the type of the donor atoms and the stability of the Ga(III) complexes. Additionally, the complexation can protect the Ga(III) ion against hydrolysis, and thus the formation of kinetically more inert gallate, and can modify the hydrophilic–lipophilic character as well [12, 13]. Therefore, the distinct pharmacokinetics of the gallium salts compared with that of the complexes is based on their different physical–chemical properties. As a consequence, the $Ga(NO_3)_3$ is rapidly excreted in the urine owing to hydrolysis at physiological pH [3, 12], whereas almost all Ga(III) is reported as being bound to Tf, providing a prolonged lifetime and higher therapeutic index in the case of GaM [12]. KP46 has much greater stability than GaM, which is reflected in its approximately eight orders of magnitude higher log β value, which results in negligible decomposition at physiological pH even in the biologically relevant low concentration range [14]. Thus, KP46 is able to preserve its original form more considerably than other Ga(III) complexes [14]. In addition, KP46 has a relatively high lipophilic character, which is an important issue when transport protein binding is considered. Only a few data can be found in the recent literature on the interaction of KP46 with serum proteins [10, 15–17], since such investigations are very often hampered by the low aqueous solubility of KP46 (36 μM [15]), and this can be a reason why the data are not congruent. A capillary electrophoresis–mass spectrometry method was used to study the interaction between KP46 and Tf or human serum albumin (HSA), and the metal ion was found to bind to Tf exclusively and only a low affinity toward HSA was observed [10]. On the other hand, X-ray absorption spectroscopy studies showed that the coordination environment of the metal center remains intact in the presence of human serum apotransferrin (apoTf) or HSA, and Hummer et al. [16] suggested that the interaction mechanism is based on a noncovalent, more hydrophobic binding. HSA is the most abundant blood plasma protein (630 μM) and has nonspecific binding pockets where chemically diverse endogenous and exogenous compounds can bind [18]. Interaction with HSA has a serious impact on the pharmacokinetic profile of many drugs. In addition, the accumulation of HSA and HSA-bound drugs in solid tumors as a consequence of an enhanced permeability and retention effect can be an operative way of selective tumor targeting [19].

To make the clinical studies of the promising Ga(III) complexes with antitumor activity more straightforward, the role of the serum proteins in the drug delivery should be considered in addition to establishing their mechanism of action in detail, such as identifying the target cellular proteins of KP46 [17]. In the light of the utmost importance of HSA and Tf binding in the distribution and transportation of drugs, a detailed comparative study of the interaction between these serum proteins and both Ga(III) complexes (KP46 and GaM) undergoing clinical trials was performed in pure aqueous solution in the present work. Beside these two proteins, the effect of additional low molecular mass (LMM) bioligands on the speciation was investigated. Techniques such as fluorometry, UV–vis spectrophotometry, ^{1}H and saturation transfer difference (STD) NMR spectroscopy, and membrane ultrafiltration–UV–vis spectrophotometry were applied to characterize the binding events and to provide a quantitative description of the systems studied. Modeling calculations were performed to describe the species distribution of Ga(III) complexes in blood serum with the aid of the conditional

stability constants. The experimental data are complemented by protein–complex docking calculations.

Results and discussion

Interaction of KP46 and GaM with LMM serum components

Solution equilibrium studies in our previous work [14] revealed that the tris(ligand) Ga(III) complexes of both 8-hydroxyquinoline (HQ) and 3-hydroxy-2-methyl-4*H*-pyran-4-one (maltol) predominate at physiological pH in aqueous solution. Since KP46 possesses an approximately eight orders of magnitude higher overall stability constant than GaM, it has the ability to preserve its original form much more strongly against the effect of dilution or competitor ligands compared with the maltolato complex. Therefore, significantly different biodistribution processes are expected when these Ga(III) complexes are administered to a living organism.

The original form of the metallodrug tris complexes GaM and KP46 can be changed in the extracellular or intracellular biological fluids by biotransformation processes, and the carrier ligands may be partly or completely displaced by suitable endogenous Ga(III) binders. In the bloodstream, interaction with both low molecular mass (LMM) and high molecular mass (HMM) molecules should be considered when the extent to which the complexes are able to retain their original forms is in question. According to the hard Lewis acid character of Ga(III), chelating agents with oxygen donor atoms present in serum such as citrate, phosphate, oxalate, and hydroxide are the primary candidates among the LMM compounds to compete with the original ligands, similarly to the case of Al(III) [20]. Additionally, the rate of binding of Ga(III) ion or Ga(III) complexes to LMM compounds is expected to be higher than that to larger bioligands. Therefore, the effect of citrate, phosphate, and oxalate on the UV–vis spectra of GaM and KP46 was followed first. No measurable spectral changes were detected in the presence of these LMM binders neither at their serum concentrations nor at tenfold higher concentrations, suggesting that the original ligands of both Ga(III) complexes are not replaced by these compounds (Fig. S1).

It is noteworthy that all the measurements in this work were performed at 25 °C as most of the stability constants used for the modeling calculations published in the literature were determined at this temperature.

Interaction of KP46 and GaM with HSA

HSA acts as the most important transport "vehicle" for a wide variety of endogenous and exogenous ligands, metal ions, and metal complexes, and provides different types of binding modes [18]. Namely, available donor species of the protein such as the free thiol (Cys34) and imidazole nitrogens (His) are able to coordinate to metal ions in a monodentate mode; in addition, HSA has well-defined metal binding moieties (N-terminal and multimetal binding sites) where the simultaneous presence of four donor atoms can be found, which can host mainly bivalent metal ions such as Cu(II), Zn(II), Ni(II), and V(IV)O [21]. On the other hand, HSA displays extraordinary ligand binding properties, and van der Waals forces, hydrogen bonding, and electrostatic and hydrophobic interactions are involved in the stabilization of the protein–ligand adducts at two main binding sites located in subdomain IIA (site IIA) and subdomain IIIA (site IIIA) [18, 22]. According to the conventional view based on Sudlow's classification [22, 23], these sites are known as site I, which is a large, hydrophobic multichamber cavity for usually bulky negatively charged heterocyclic compounds, and site II, which has high affinity for small aromatic compounds typically containing a peripheral negative charge, respectively [24–27]. A third binding pocket within subdomain IB (site IB) has recently been identified as the primary or secondary binding site of various pharmaceutical drugs and natural compounds such as a bilirubin photoisomer, lidocaine, and hemin [27]. HSA also offers the possibility of dissolution in serum for highly hydrophobic compounds. On the basis of these binding characteristics of HSA, the formation of protein–metallodrug adducts is expected in the case of KP46 and GaM instead of competition with the ligands for the Ga(III) ion.

Firstly, ^{1}H NMR spectra of GaM in the absence or the presence of HSA were recorded at pH 7.4 and compared (Fig. S2). The spectrum of GaM shows that the complex is partly decomposed and approximately 5 % of the maltol is not bound under the given conditions (gallium-to-maltol ratio of 1:3, $c_{Ga} = 1$ mM), which corresponds well with the expectations [14]. In the presence of this serum protein, the ratio of the Ga(III)-bound ligand and the free form of the ligand is almost unchanged, and only the peaks belonging to the free form of the ligand show electronic shielding effects—namely, an upfield shift of the peaks is seen, whereas the positions of the peaks of the tris complex are constant. These observations suggest that there is no measurable interaction between HSA and GaM, although maltol is able to bind weakly, which was proved in our former work [28]. Practically no binding of GaM was found as well when ultrafiltration–UV–vis measurements were performed as the spectra of the LMM fractions of the GaM–HSA system following the separation were fairly similar to the reference spectra of GaM (Fig. S3). (The minor difference between the spectra originated from the weak binding of the ligand to the protein).

Since KP46 exhibits significant intrinsic fluorescence [14], its interaction with HSA could be investigated by fluorometry. Addition of HSA to the metal complex increased its emission intensity significantly (Fig. 1a), and the emission maximum was also shifted to lower wavelengths. The equilibrium was always reached quickly (within 15–20 min). HSA emits weakly at the applied excitation wavelength (λ_{ex} = 367 nm), which had to be taken into consideration during the data evaluation, although the measured intensity at each titration point was found to be always much higher than the sum of the intensities of HSA and KP46 alone (Fig. 1b). These findings point out the unambiguous interaction between the Ga(III) complex and the protein. A conditional stability constant of log K' = 4.04 ± 0.08 was calculated for the HSA–KP46 species on the basis of the deconvolution of the recorded emission spectra, indicating a moderate binding strength (see details in "Materials and methods"). It is noteworthy that only a low extent of adduct formation was reported by Groessl et al. [10] at 50 μM HSA and 20 μM KP46; however, approximately 30 % of the complex is expected to be bound to HSA on the basis of our binding constant under the conditions applied.

In addition, STD NMR measurements were performed for the HSA–KP46 system; STD NMR spectroscopy is a useful technique for studying dynamic protein–ligand interactions, since structural information is obtained noninvasively without requiring separation. In this experiment, the saturation of the protein is spread onto the small compound owing to the binding and the signal intensity of the ligand (or complex) is attenuated. Subtraction of the spectrum obtained from the reference spectrum of the small compound without saturation results in the STD NMR spectrum, and therefore only binder molecules exhibit STD NMR spectra [29]. Since KP46 has quite low water solubility, the ^{1}H and STD NMR spectra were recorded at 20 μM by a 600-MHz spectrometer equipped with a cryoprobe (Fig. 2) in order to obtain well-detectable signals.

In the ^{1}H NMR spectrum of KP46, signals of nonequivalent ligand protons were detected, revealing the coexistence of structural isomers of the Ga(III) complex in solution. The STD signals measured for the KP46–HSA system corroborate the binding of the complex to the protein. The similar character of the ^{1}H and STD NMR spectra suggests that the complex does not decompose in the presence of HSA, the original ligand HQ is not replaced, and thus the coordination mode around Ga(III) is retained. The unchanged metal center of KP46 in the presence of HSA was also found by X-ray absorption spectroscopy measurements [16].

The UV–vis and fluorescence difference spectra calculated for the HSA–HQ system at pH 7.4 (Fig. S4) led to the conclusion that the ligand is also able to bind to this

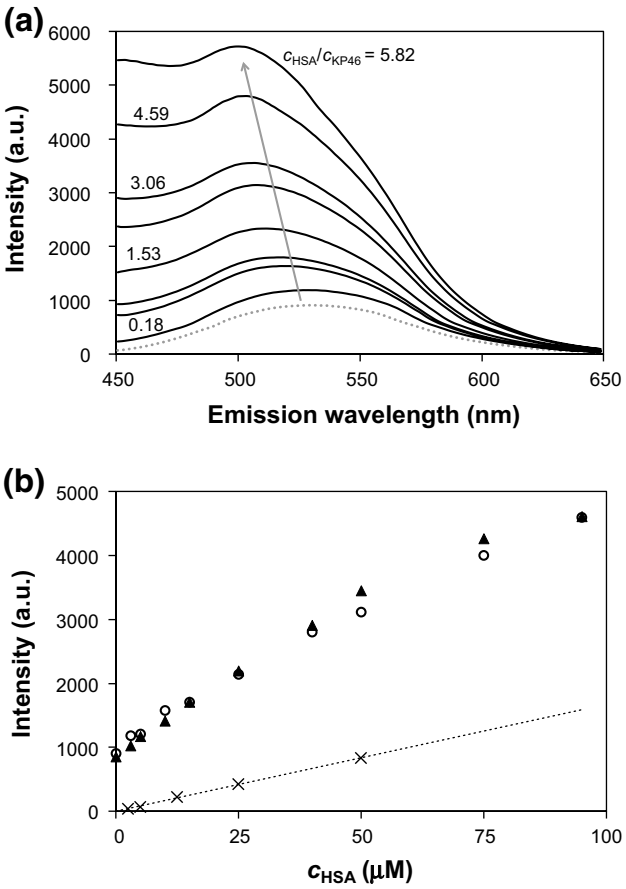

Fig. 1 **a** Fluorescence spectra of KP46 alone (*dotted line*) and KP46 when titrated with human serum albumin (HSA; *solid lines*). **b** Changes of the fluorescence intensities of KP46–HSA-containing samples (*triangles*, *circles* parallel measurements) and HSA alone (*crosses*) at 532 nm versus c_{HSA}. c_{KP46} = 16 μM, c_{HSA} = 3–95 μM, λ_{ex} = 367 nm, pH 7.4, 25 °C

serum protein weakly, although the data collected could not be evaluated quantitatively owing to the strong noise. Considering the prominent high stability of KP46, the interaction occurring between its ligand and HSA is not expected to have a significant effect on the distribution of the metallodrug in serum.

Although both GaM and KP46 are neutral compounds, only KP46 shows measurable binding affinity toward HSA, most probably owing to its more lipophilic character (log *P* 0.88 for KP46 [15] vs 0.41 for GaM [3]) and the aromatic nature of the coordinating ligands, which can provide stacking interactions with the protein. The quite low water solubility of KP46 hinders the application of the ultrafiltration method, and studying the displacement reactions with the use of well-established site marker compounds (such as warfarin and dansylsarcosine) was not advantageous owing to the significant emission of the complex. To obtain deeper insight into the binding event, molecular modeling studies

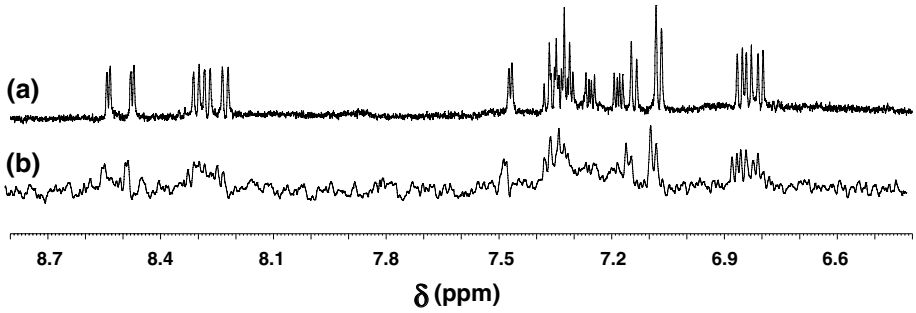

Fig. 2 ^{1}H NMR spectrum of KP46 (*a*) and saturation transfer difference NMR spectrum of KP46 in the presence of HSA (*b*). $c_{KP46} = 20$ μM, $c_{HSA} = 5$ μM, pH 7.4, 7 °C, 10 % (v/v) D_2O

were performed in which KP46 was analyzed by means of studies of docking into the crystallographic structure of HSA.

Molecular modeling studies for the interaction of KP46 with HSA

To suggest a possible binding mode for KP46, its interaction toward HSA was analyzed in depth by means of docking evaluation. Three different crystallographic structures of HSA were used to analyze the binding interaction of KP46, and a blind docking evaluation was performed. KP46 was docked on the whole surface of the three X-ray HSA structures by means of AutoDock4 [30], resulting in 1,000 different poses collected for each protein. All the docking poses were clusterized on the basis of their disposition, and the clusters populated with at least 90 docking poses were analyzed (corresponding to 3 % of the total docking poses). As shown in Fig. 3a, about 1,300 of the 3,000 evaluated docking poses identified a particular region of HSA as the most probable for the interaction with KP46. Furthermore, this cluster (CL1) was also the one with the highest average energy interaction value between KP46 and the target protein. The analysis of the docking disposition of the conformers belonging to this cluster supported the possible interaction of KP46 into the IB binding site (Fig. 3b).

Owing to the large cluster population of CL1 (see Fig. 3), this disposition was considered as the most reliable. To further confirm the geometries obtained and to further analyze the ligand–protein interactions, a quantum mechanical/molecular mechanical ONIOM approach [31] was applied to the starting docking of KP46 into the IB binding site. Figure 4 shows the resulting HSA–KP46 adduct; the binding site surface analysis highlighted that two of the three HQ rings were inserted into two lipophilic subcavities, whereas the third HQ ring was solvent exposed and surrounded by charged residues (Fig. 4a). In more detail, one of the three HQ ligands was inserted into a subcavity mainly delimited by L139, I166, and Y185, whereas the other lipophilic subcavity in which the other HQ moiety interacted was mainly delimited by Y162, F173, L178, F181, L206, and L212 (Fig. 4b). Finally, the third

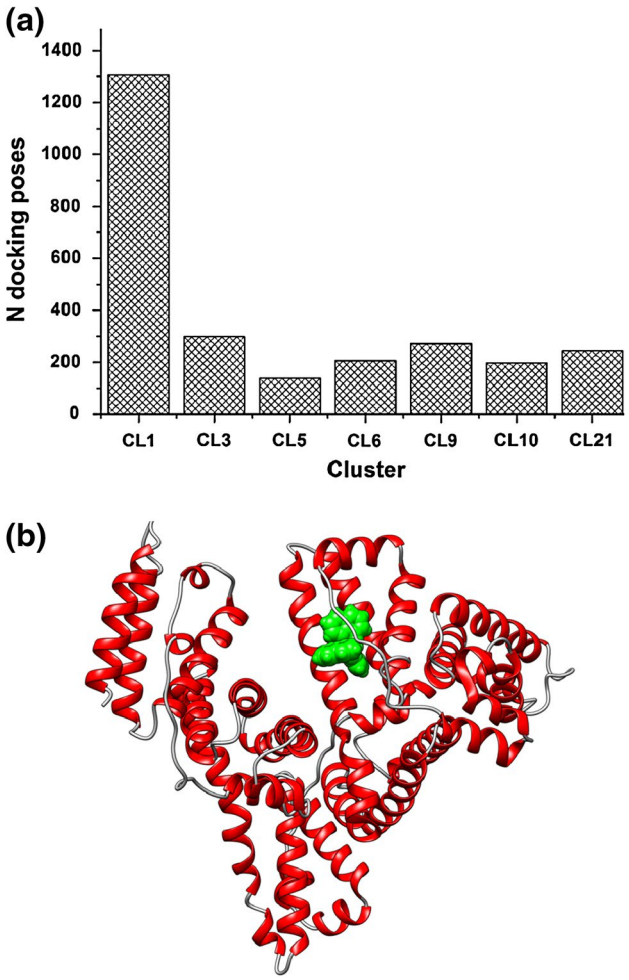

Fig. 3 Number of docking poses for the highest populated docking clusters (**a**) and binding interaction region corresponding to CL1 (**b**) for the KP46–HSA system

HQ ligand was solvent exposed and surrounded by R138, R169, H170, R210, and K214.

Interaction of KP46 and GaM with Tf

It is well known from the literature that Tf binds Ga(III) at the Fe(III) binding site,s and the conditional binding

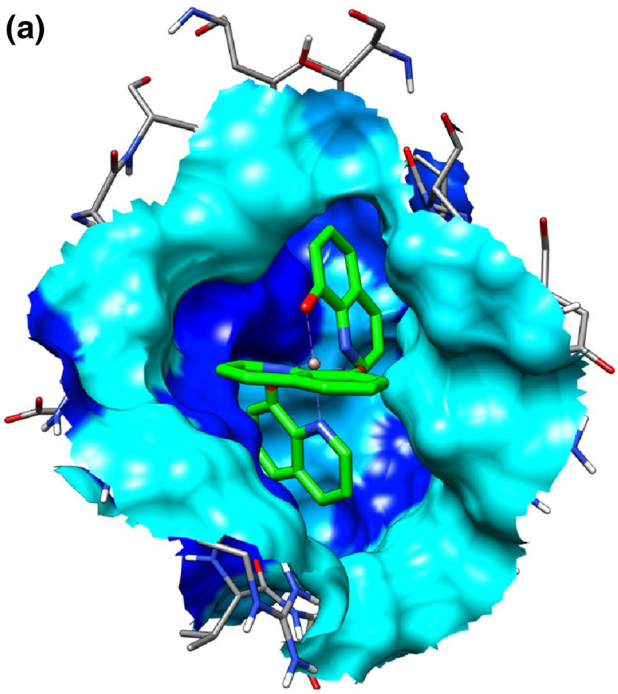

Fig. 4 Molecular surface (**a**) and residue analysis (**b**) of the HSA binding site for KP46. The surface is colored according to the Kyte–Doolittle hydrophobicity scale (*blue* for the high and *sky blue* for the low Kyte–Doolittle hydrophobicity values)

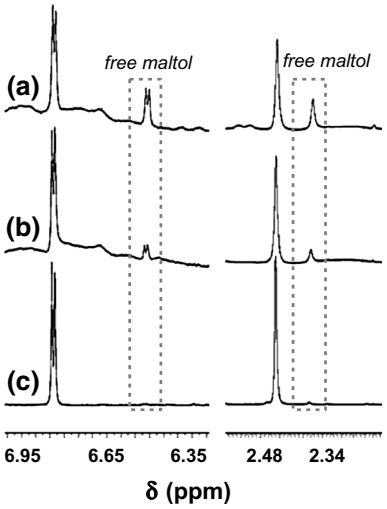

Fig. 5 ^{1}H NMR spectra of the GaM–apotransferrin (apoTf) system in the presence of 25 mM HCO_3^- (*a*) and without it (*b*) and GaM alone (*c*). c_{GaM} = 1.0 mM, c_{apoTf} = 0.5 mM, c_{NaHCO3} = 25 mM, pH 7.4, 25 °C, 10 % (v/v) D_2O

constants are log $K_1' = 20.3$ and log $K_2' = 19.3$ at pH 7.4, and carbonate acts as a synergistic anion [32]. Tf is considered as the predominant chelating agent for the binding and transport of Ga(III) in human serum [12]; therefore, Tf is an essential competitor in the case of Ga(III) complexes, and during the application of these metallodrugs, a crucial question, with regard to their efficiency and mechanism of action, is the actual chemical form in which they can be found in serum. Owing to the much higher stability of KP46 compared with GaM, a different level of ligand displacement is expected for Tf.

Interaction between GaM and apoTf was monitored by UV–vis spectrophotometry, ^{1}H NMR spectroscopy, and fluorometry. As a first step, difference UV–vis spectra were recorded at various protein-to-GaM ratios at physiological pH (Fig. S5), in order to obtain preliminary information on whether there is interaction between them. Considerable concentration-dependent absorbance-difference values were obtained, most probably owing to the competition between apoTf and maltol for Ga(III). The ligand displacement by the protein, and thus the liberation of maltol, could be clearly seen in the ^{1}H NMR spectra (Fig. 5), and in the presence of hydrogencarbonate, much more free maltol was detected in accordance with our expectations.

ApoTf possesses intrinsic fluorescence mainly due to Tyr and Trp residues, and both are excited at 280 nm [33]. The distorted octahedral metal ion binding sites of apoTf consist of the donor atoms of four amino acids (Asp, Tyr, Tyr, His) beside the synergistically bound bidentate carbonate [32, 34, 35]. The emission intensity is usually quenched on the coordination of the Tyr residues to metal ions [33], and thus the decrease of the signal can be used to follow the interaction. Fluorescence titration of apoTf by addition of GaM (Fig. 6) and $GaCl_3$ for comparison was performed at pH 7.4 in the presence of 25 mM HCO_3^-. The equilibrium

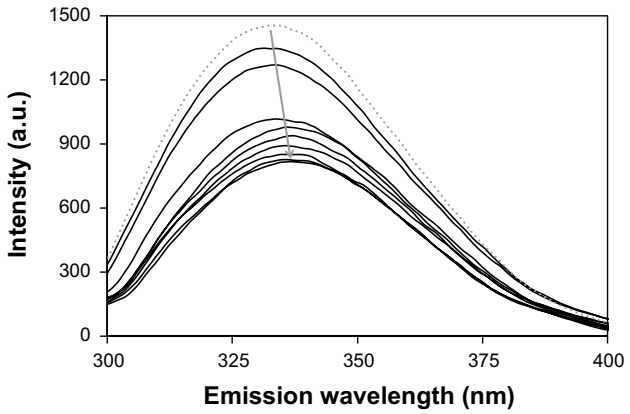

Fig. 6 Fluorescence spectra of apoTf (*dotted gray line*) and apoTf titrated with GaM (*solid black lines*). c_{apoTf} = 0.2 μM, c_{GaM} = 0.2–4 μM, λ_{ex} = 280 nm, pH 7.4, 25 °C

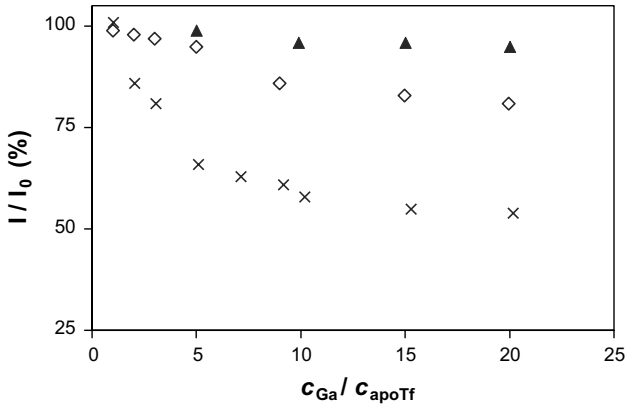

Fig. 7 Changes of the fluorescence intensities of apoTf with addition of GaM (*crosses*), KP46 (*diamonds*), and $GaCl_3$ (*triangles*) at 340 nm versus c_{Ga}/c_{apoTf}. c_{apoTf} = 0.2 μM and $c_{complex}$ = 0.2–4 μM for GaM and KP46, c_{apoTf} = 2 μM and c_{GaCl3} = 20–100 μM for $GaCl_3$, λ_{ex} = 280 nm, pH 7.4, 25 °C

was reached within 20–25 min in the case of GaM. When the concentration of GaM in the samples was increased, the emission intensity diminished significantly (Fig. 7) as a result of the displacement of maltol by the donor atoms of the protein in the coordination sphere. At the same time, addition of the Ga(III) salt to the protein did not decrease the intensity even at tenfold excess and during 4 h of incubation (Fig. 7). Ga(III) tends to hydrolyze strongly, and significant amounts of anionic gallate are present in solution at physiological pH without the protection of coordinating ligands [36].

Formation of the Ga(III)–apoTf complex in the $[Ga(OH)_4]^-$-containing system is fairly slow, which leads to the rapid excretion of Ga(III) salts by the kidneys [3, 12]. In the case of GaM, interaction with apoTf is much faster, and the administered Ga(III) is reported to be bound to the protein, providing the possibility for the Tf-dependent gallium uptake mechanism [12]. However, the extent of the displacement of the carrier ligand by the protein strongly depends on the actual concentration of GaM in the serum. Therefore, distribution curves were computed with the aid of the binding constants of the Ga(III) complexes formed with maltol [14], hydroxide [36], and apoTf [32] at various total concentrations of the metallodrug assuming that approximately 30 % of the metal binding sites are occupied by ferric ions (Fig. 8a). Our modeling calculations show that maltol is completely replaced at a concentration below 30 μM and only half of the GaM is able to keep its original form at 100 μM.

Similar modeling calculations were performed for the KP46–apoTf system on the basis of the stability data [14, 32, 36] (Fig. 8b), and revealed that the ligand HQ keeps Ga(III) bound much more efficiently than maltol owing to the higher stability of KP46 compared with GaM. Tyr emission quenching experiments support this finding

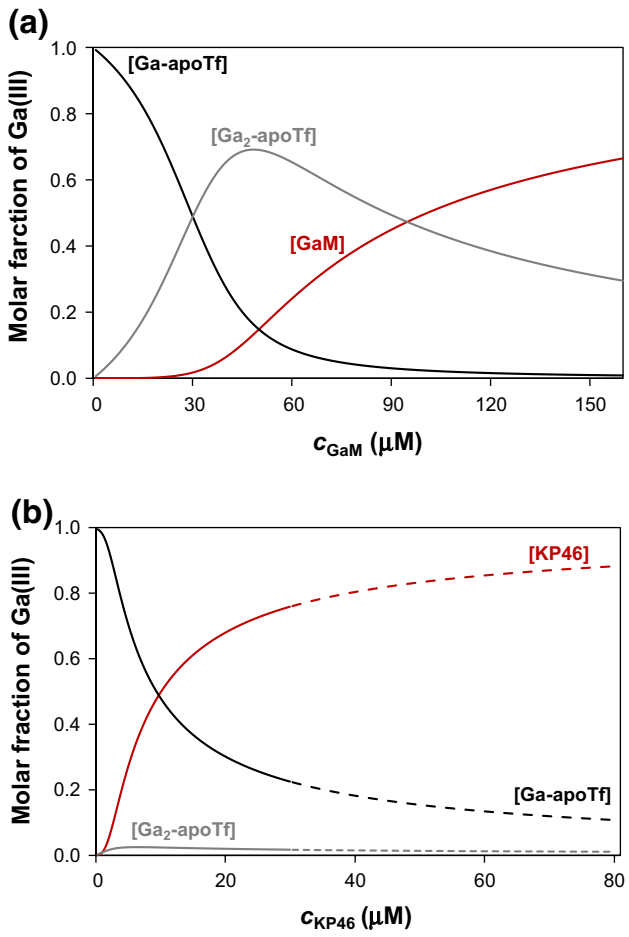

Fig. 8 Concentration distribution curves for the GaM−apoTf (**a**) and KP46−apoTf (**b**) systems as a function of the total concentrations of the complexes. *Dashed lines* denote KP46 concentrations over the solubility limit. c_{apoTf} = 37 μM considering that 30 % of the binding sites on apoTf are saturated with Fe(III), pH 7.4

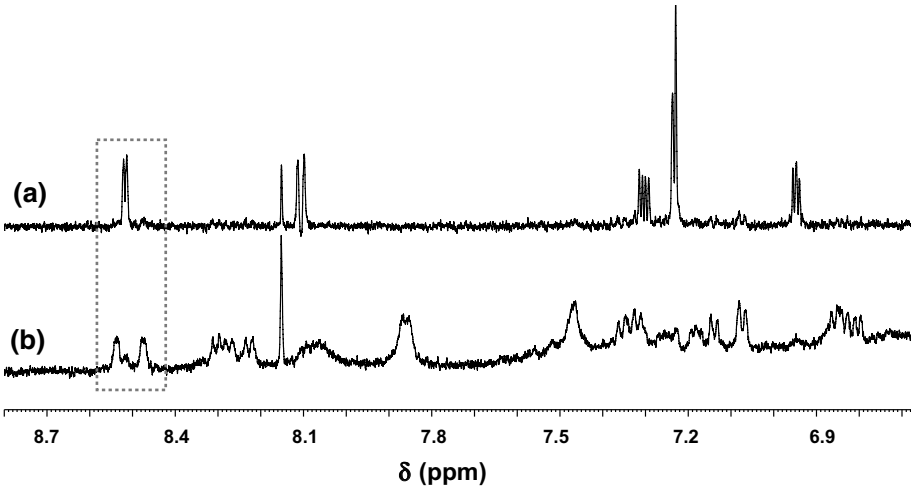

Fig. 9 ^{1}H NMR spectra of 8-hydroxyquinoline (HQ) alone (*a*) and KP46 together with apoTf (*b*). (For KP46 alone for comparison, see Figs. 2a and S6). $c_{HQ} = 60$ μM, $c_{KP46} = 20$ μM, $c_{apoTf} = 20$ μM, $c_{NaHCO3} = 25$ mM, pH 7.4, 7 °C, 10 % (v/v) D_2O

as the decrease of the measured intensity, and thus the extent of binding of Ga(III) to apoTf, was significantly lower in the case of KP46 (Fig. 7). Interaction of KP46 with apoTf was also monitored by ^{1}H NMR spectroscopy at low concentration (20 μM; Figs. 9, S6). The spectrum recorded in the presence of the protein clearly shows the partial release of the ligand HQ, and the ratio of the areas of the corresponding peaks of the bound HQ and nonbound HQ could be estimated and converted to molar fractions. Namely, approximately 71 % of HQ is bound to Ga(III) under the conditions applied, which corresponds well with the value of 70 % calculated using the stability constants.

The fluorogenic property of HQ by which the fluorescence intensity is enhanced by the coordination to Ga(III) is well known from the literature, and this feature allowed us to determine the overall stability constants of the complexes formed in the Ga(III)–HQ system in pure aqueous solution by fluorometry in our former work [14]. As the emission intensity of the bound ligand is ten times stronger than that of the free form of the ligand, the displacement of HQ by apoTf can be followed by this technique as well. Therefore, fluorescence spectra of KP46 were recorded in the absence and in the presence of apoTf using an incubation time of 1 h (as equilibrium could be reached within this time frame), and the measured intensities were compared (Fig. 10). It is noteworthy that apoTf does not emit when excited at the excitation wavelength applied (367 nm), and only KP46 and the free HQ contribute to the measured signal. It is seen that in the presence of the protein the intensity is decreased, and the equilibrium concentration of the unchanged KP46 could be calculated from the measured intensities at each titration point and then the quantity of the metal ion bound to the protein could be estimated (Fig. 11). On the other hand, these concentration data could be also computed using the stability constants. The results

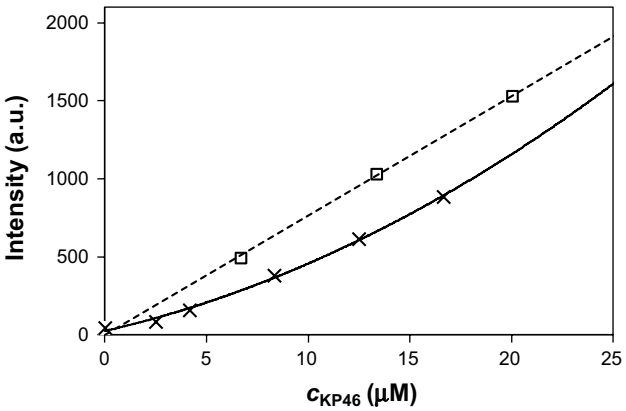

Fig. 10 Fluorescence intensities measured in the KP46−apoTf system (*crosses*) and for KP46 alone (*squares*) at 532 nm versus c_{KP46}. $c_{apoTf} = 25$ μM, $c_{KP46} = 2.5$-20 μM, $\lambda_{ex} = 367$ nm, pH 7.4, 25 °C

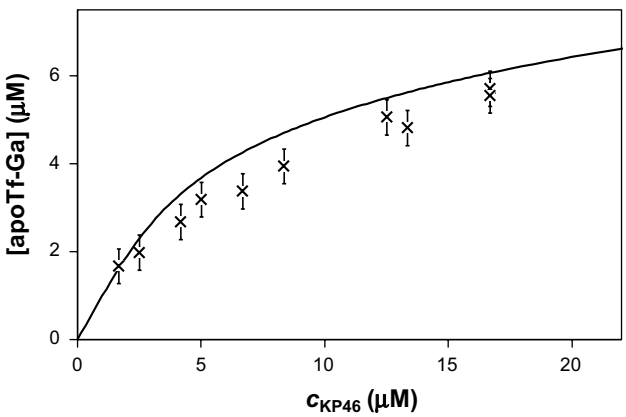

Fig. 11 ApoTf-bound Ga(III) equilibrium concentrations calculated on the basis of the deconvolution of the fluorescence spectra recorded for the apoTf−KP46 system (*crosses*) together with the simulated curve obtained using various binding constants (*line*). $c_{apoTf} = 25$ μM, $c_{KP46} = 2.5$–17 μM, pH 7.4, 25 °C

demonstrate strong correlation between the data obtained by modeling calculations and experiments (Fig. 11).

Predicted distribution of KP46 and GaM in serum

Finally, multicomponent equilibrium modeling calculations were performed in order to predict the actual chemical forms of the studied Ga(III)-containing metallodrugs in human serum. Knowledge of the speciation and the most plausible chemical forms of these complexes in aqueous solution under physiological conditions is a mandatory prerequisite for understanding the alterations in their pharmacokinetics and mechanism of action. Thus, distribution curves were computed for the KP46 (Fig. 12) or GaM (Fig. S7) complexes in the presence of Tf (37 μM) and HSA (630 μM) at physiological pH, and conditional stability constants of the following adducts were used: Ga(III) complexes formed with the carrier ligand (HQ or maltol) [14]; Ga–apoTf, Ga_2–apoTf [32]; KP46–HSA (determined in this work); maltol–HSA [28]; and various Ga(III)–hydroxido complexes [36]. A typical 30 % saturation of the two metal binding sites of Tf with ferric ions is assumed. First, it can be concluded that the species distribution strongly depends on the actual analytical concentrations of the Ga(III) complexes. In the case of the GaM complex in the biologically relevant concentration range (up to approximately 160 μM [12]), displacement of maltol by Tf, and thus formation of Ga(III) complexes of this protein, is observed and is more pronounced with decreasing concentration of GaM and is complete at concentrations lower than approximately 30 μM. HSA is able to bind weakly the carrier ligand maltol, but its effect on the distribution in the concentration interval studied is minor (Fig. S7). In contrast, the role of Tf in the distribution of KP46 is much less significant owing to the prominent stability of this metal complex which hinders the displacement of HQ by the protein, whereas HSA is responsible for the binding of most of the complex (Fig. 12).

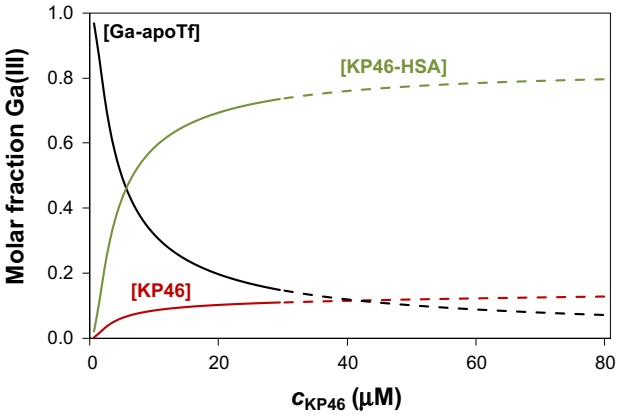

Fig. 12 Concentration distribution curves for the KP46–Tf–HSA system as a function of the analytical concentrations of KP46. *Dashed lines* denote the KP46 concentration range over the solubility limit. $c_{HSA} = 630$ μM, $c_{Tf} = 37$ μM considering that 30 % of the binding sites on Tf are saturated with Fe(III), pH 7.4

Conclusions

Numerous drugs are known to be bound to plasma proteins when they enter the bloodstream, and reactions of anticancer metallodrugs with these proteins are of considerable interest as they have a profound effect on the biodistribution, the toxicity, the side effects, and even the mechanism of action. A panel of methods comprising spectrofluorometry, UV–vis spectrophotometry, ^{1}H and STD NMR spectroscopy, and membrane ultrafiltration–UV–vis spectrophotometry at 25 °C in addition to in silico calculations were used to study the interactions of KP46 and GaM with HSA and apoTf. The role of some LMM serum components (citrate, phosphate, and oxalate) as potential Ga(III) binders in the distribution was also checked, and no influence was found under serum conditions. ApoTf is able to compete for Ga(III) with the carrier ligands of the complexes studied depending on their total concentrations, although substitution of maltol occurs to a much higher extent compared with that of HQ. Replacement of HQ by apoTf could be followed by fluorometry, and the data were evaluated quantitatively, with the results supporting the modeling calculations based on the stability constants. A moderate binding of KP46 to HSA was proved ($\log K' = 4.04$; $K_D = 91$ μM) by the use of fluorometric and STD NMR measurements. Modeling calculations confirmed the interaction which occurs most likely at the IB binding site. Negligible influence of HSA was found on the distribution in the case of GaM. Equilibrium modeling calculations on the speciation of the Ga(III) complexes in the presence of Tf and HSA were performed, and an unambiguously different distribution was obtained. Although stability data obtained at 25 °C were used for the calculations, similar but not identical speciation curves are expected at 37 °C. It was found that in the case of GaM the role of Tf is significant and the protein is able to replace maltol completely at concentrations lower than 30 μM. In contrast, primarily binding of KP46 to HSA is predicted under physiological conditions, which may be advantageous with respect to increased solubility and half-life. It is noteworthy that the binding to HSA is reversible and does not alter the original coordination mode in the complex. These findings also suggest a Tf-independent gallium uptake mechanism for KP46 parallel to or instead of the Tf-receptor-mediated endocytosis pathway.

Materials and methods

Chemicals

Maltol, HQ, $GaCl_3$, HSA (as lyophilized powder with fatty acids, A1653), apoTf (T2036), KCl, $NaHCO_3$, citric acid, oxalic acid, 4-(2-hydroxyethyl)-1-piperazineethanesulfonic acid (HEPES), Na_2HPO_4, and NaH_2PO_4 were obtained from Sigma-Aldrich in puriss quality. Double-distilled Milli-Q water was used for sample preparations.

HSA and apoTf solutions were freshly prepared before the experiments, and their concentrations were estimated from their UV absorption: $\varepsilon_{280\ \mathrm{nm}}(\mathrm{HSA}) = 36{,}850\ \mathrm{M^{-1}\ cm^{-1}}$, $\varepsilon_{280\ \mathrm{nm}}(\mathrm{apoTf}) = 92{,}300\ \mathrm{M^{-1}\ cm^{-1}}$ [37]. $GaCl_3$ stock solution was prepared in HCl. Its concentration was determined by complexometry via the EDTA complexes. Accurate strong acid content of the Ga(III) stock solution was determined by pH-potentiometric titrations. GaM and KP46 stock solutions were prepared in the appropriate buffer solution by mixing the Ga(III) ion and the ligand-containing solutions, resulting in a 1:3 metal-to-ligand ratio.

Spectrofluorometric measurements

Fluorescence spectra were recorded with a Hitachi-F4500 fluorimeter using 5 nm/5 nm, 5 nm/10 nm, and 10 nm/10 nm slit widths in a 1-cm quartz cell at 25.0 ± 0.1 °C. All solutions were prepared in 10 mM HEPES buffer (pH 7.4) containing 100 mM KCl and were incubated for 1 or 2 h. Samples usually contained 1–95 μM HSA, and various HSA-to-ligand (or metal complex) ratios (from 1:0 to 1:30) were used. The samples of apoTf always contained 25 mM $NaHCO_3$. The excitation wavelengths were 280, 295, or 367 nm depending on the type of experiment, and the emission was read in the range from 290 to 650 nm. Two or three parallel experiments were performed for each sample.

A correction for self-absorbance was sometimes necessary in the experiments when the fluorescence was significantly absorbed by the samples. The correction was done according to the following equation [38]:

$$I_{\mathrm{corrected}} = I_{\mathrm{measured}} \times 10^{(A(\mathrm{EX})+A(\mathrm{EM}))/2},$$

where $I_{\mathrm{corrected}}$ and I_{measured} are the corrected and measured fluorescence intensities, and A_{ex} and A_{em} are the absorptivities at the excitation and emission wavelengths in the samples, respectively. The conditional binding constant for the HSA–KP46 adduct was calculated with the computer program PSEQUAD [39]. Calculations were based on the chemical equilibrium

$$p\,(\mathrm{KP46}) + q\,(\mathrm{HSA}) \rightleftharpoons \left[(\mathrm{KP46})_p(\mathrm{HSA})_q\right];\ \beta'_{pq} = \left[\left[(\mathrm{KP46})_p(\mathrm{HSA})_q\right]\right]/[\mathrm{KP46}]^p[\mathrm{HSA}]^q;$$

and mass balance equations

$$c_{\mathrm{KP46}} = [\mathrm{KP46}] + \sum_{i=1}^{n} p_i\beta'_{pq}[\mathrm{KP46}]^{p_i}[\mathrm{HSA}]^{q_i};\ c_{\mathrm{HSA}} = [\mathrm{HSA}] + \sum_{i=1}^{n} q_i\beta'_{pq}[\mathrm{KP46}]^{p_i}[\mathrm{HSA}]^{q_i},$$

where β'_{pq} is the overall conditional binding constant of the HSA–KP46 complex, and c_x and [x] are analytical (total) and equilibrium concentrations of component x, respectively. The best fit of the experimental data to the calculated data was obtained when p and q were both assumed to be 1 (as the KP46–binding site reaction follows one-to-one stoichiometry). The measured fluorescence intensities (I_i at i nm) are proportional to the equilibrium concentrations, where ϕ^i_x is the proportionality constant (i.e., "molar intensity") of component x at i nm:

$$I_i = \Phi^i_{\mathrm{KP46}} \times [\mathrm{KP46}] + \Phi^i_{\mathrm{HSA}} \times [\mathrm{HSA}] + \Phi^i_{[\mathrm{HSA-KP46}]} \times [[\mathrm{HSA} - \mathrm{KP46}]].$$

Membrane ultrafiltration–UV–vis measurements

Samples were separated by ultrafiltration through 10-kDa membrane filters (Microcon YM-10 centrifugal filter unit, Millipore) in LMM and HMM fractions with the help of a temperature-controlled centrifuge (Eppendorf MiniSpin plus, 12,000 revolutions per minute, 10 min). The samples (0.50 mL) contained 200 μM HSA and GaM (from 50 to 150 μM) in 10 mM HEPES buffer (0.1 M KCl; pH 7.4 at 25.0 ± 0.1 °C) and were incubated for 1 h. The LMM fraction containing the nonbound metal complex was separated from the protein and protein adducts in the HMM fraction. The LMM fractions were then diluted to known volumes, and the concentration of the nonbound complex was determined by UV–vis spectrophotometry. The UV–vis spectra of the LMM fractions were compared with the reference spectra of the samples containing GaM without the protein at a concentration equal to that in the diluted, ultrafiltered samples.

UV–vis spectrophotometric measurements

A Hewlett-Packard 8452A diode-array spectrophotometer was used to record the UV–vis spectra in the interval from 200 to 800 nm at 25.0 ± 0.1 °C and with a path length of 1 or 2 cm in the case of HQ-containing samples. Measurements were performed at 20–37 μM protein concentrations, and various protein-to-complex ratios (from 1:0 to 1:5) were used. All samples were prepared in 10 mM HEPES buffer (pH 7.4) containing 0.1 M KCl (together with 25 mM $NaHCO_3$ in case of the apoTf) and were incubated for 1 or 2 h. Difference UV–vis spectra for the

HSA–HQ system were obtained for samples containing 20 μM HSA and 20–160 μM HQ, and spectra of reference samples were recorded under the same conditions without the protein.

NMR measurements

^{1}H NMR spectra were recorded with a Brucker Ultrashield 500 Plus instrument at 25 °C. The proteins and GaM were dissolved in a 10 % (v/v) D_2O and H_2O mixture containing 20 mM HEPES (pH 7.4) and 0.1 M KCl to yield concentrations of 0.5 and 1 mM, respectively. Chemical shifts (δ) are reported in parts per million from 4,4-dimethyl-4-silapentane-1-sulfonic acid. All ^{1}H NMR spectra were recorded with the WATERGATE water suppression pulse scheme using 4,4-dimethyl-4-silapentane-1-sulfonic acid as an internal standard.

^{1}H (for KP46) and STD NMR measurements were performed using a 600 MHz Bruker Avance III spectrometer equipped with a 5 mm cryo-TXI (^{1}H, ^{13}C, ^{15}N) probe with *z*-gradient at 7 °C. The protein and HQ (or KP46) were dissolved in 20 mM phosphate buffer [pH 7.4, 10 % (v/v) D_2O and H_2O] and an incubation time of 24 h was applied. Spectra were acquired with the water suppression using excitation sculpting with pulsed gradients scheme. For the ^{1}H and STD measurements, the HSA and the KP46 concentrations were 5 and 20 μM, respectively. The concentrations of apoTf and KP46 were the same, 20 μM, and the samples also contained 25 mM $NaHCO_3$. As a reference, STD experiments were also performed without the target, containing the ligand species alone.

STD NMR spectra were acquired using a series of 40 equally spaced 50-ms Gaussian-shaped pulses for selective saturation of the protein, with a total saturation time of 2 s and a 50-ms spinlock to suppress protein signal. The frequency of the on-resonance saturation was set at 0.6 ppm and the off-resonance saturation frequency was set at 40.0 ppm. A total of 8 k scans were collected for each pseudo-2D experiment.

Docking calculations

The 3D structure of KP46 was retrieved from the Cambridge Structural Database [40, 41]. Geometry optimization was performed by means of quantum mechanical calculations based on density functional theory methods included in Gaussian 09 [42]. The optimization step was performed using the B3LYP chemical model with an LANL2DZ basis set, a direct self-consistent field calculation, and a self-consistent field convergence criterion of 10^{-5}. The B3LYP model is a combination of the Becke three-parameter hybrid functional [43] and the Lee–Yang–Parr correlation functional (which also includes density gradient terms) [44]. Three HSA X-ray crystal structures were retrieved from the RCSB Protein Data Bank (PDB) [45]—i.e., HSA complexed with warfarin (PDB code 2BXD [46]), diazepam (PDB code 2BXD [46]), and 9-aminocamptothecin (PDB code 4L8U [47]). The three proteins were superimposed by means of Chimera [48], and then the region of interest used by AutoDock was defined in order to contain all the residues of the proteins. The ligand was submitted to 1,000 genetic algorithm runs for each HSA structure, and a clustering analysis of the resulting 3,000 docking poses was then performed by using a root mean square deviation threshold of 8 Å. The resulting clusters populated with at least 90 docking poses were taken into account.

Quantum mechanical/molecular mechanical ONIOM optimization studies

The ONIOM calculation was done using Gaussian 09 [42]. The adduct between HSA and the best docking pose of KP46, which also corresponded to the representative structure of the most populated cluster, was used as the starting structure. Two layers were considered: the first layer was constituted by the complex, whereas the second layer was constituted by the rest of the system. The first layer was analyzed by the B3LYP chemical model and the LANL2DZ basis set, whereas the second layer was analyzed through use of molecular mechanics theory and the AMBER force field. The α carbon of the residues was kept fixed during the calculations.

Acknowledgments This work was supported by the Hungarian Research Foundation OTKA projects PD103905 and PD83600, and by the European Union and the State of Hungary, cofinanced by the European Social Fund in the framework of TÁMOP-4.2.4.A/2-11/1-2012-0001 "National Excellence Program".

References

1. Jung Y, Lippard SJ (2007) Chem Rev 107:1387–1407
2. Jakupec MA, Keppler BK (2004) Curr Top Med Chem 4:1575–1583
3. Bernstein LR, Tanner T, Godfrey C, Noll B (2000) Met Based Drugs 7:33–47
4. Collery P, Keppler BK, Madoulet C, Desoize B (2002) Crit Rev Oncol Hematol 42:283–296
5. Jakupec MA, Galanski M, Arion VB, Hartinger CG, Keppler BK (2008) Dalton Trans 183–194
6. Hofheinz RD, Dittrich C, Jakupec MA, Drescher A, Jaehde U, Gneist M, Graf von Keyserlingk N, Keppler BK, Hochhaus A (2005) Int J Clin Pharmacol Ther 43:590–591
7. http://clinicaltrials.gov/ct2/show/study/NCT00050687. Accessed 21 Jan 2011
8. Bernstein LR, Hoeven JJM, Boer RO (2011) Anticancer Agents Med Chem 11:585–590
9. Narasimhan J, Antholine WE, Chitambar CR (1992) Biochem Pharmacol 44:2403–2408
10. Groessl M, Bytzek A, Hartinger CG (2009) Electrophoresis 30:2720–2727

11. Bernstein LR (2005) In: Gielen M, Tiekink BRT (eds) Metallotherapeutic drugs and metal-based diagnostic agents: the use of metals in medicine. Wiley, London, pp 259 − 277
12. Bernstein LR (1998) Pharmacol Rev 50:665–682
13. Lessa JA, Parrilha GL, Beraldo H (2012) Inorg Chim Acta 393:53–63
14. Enyedy ÉA, Dömötör O, Varga E, Kiss T, Trondl R, Hartinger CG, Keppler BK (2012) J Inorg Biochem 117:189–197
15. Rudnev AV, Foteeva LS, Kowol C, Berger R, Jakupec MA, Arion VB, Timerbaev AR, Keppler BK (2006) J Inorg Biochem 100:1819–1826
16. Hummer AA, Bartel C, Arion VB, Jakupec MA, Meyer-Klaucke W, Geraki T, Quinn PD, Mijovilovich A, Keppler BK, Rompel A (2012) J Med Chem 55:5601–5613
17. Timerbaev AR (2009) Metallomics 1:193–198
18. Fanali G, Masi A, Trezza V, Marino M, Fasano M, Ascenzi P (2012) Mol Aspects Med 33:209–290
19. Kratz F (2008) J Control Release 132:171–183
20. Harris WR (1992) Clin Chem 38:1809–1818
21. Bal W, Sokołowska M, Kurowska E, Faller P (2013) Biochim Biophys Acta 1830:5444–5455
22. Sudlow G, Birkett DJ, Wade DN (1975) Mol Pharmacol 11:824–832
23. Sudlow G, Birkett DJ, Wade DN (1976) Mol Pharmacol 12:1052–1061
24. Carter DC, Ho JX (1994) Adv Protein Chem 45:153–204
25. Peters T Jr (1985) Adv Protein Chem 37:161–245
26. He XM, Carter DC (1992) Nature 358:209–215
27. Zsila F (2013) Mol Pharm 10:1668–1682
28. Enyedy ÉA, Horváth L, Hetényi A, Tuccinardi T, Hartinger CG, Keppler BK, Kiss T (2011) Bioorg Med Chem 19:4202–4210
29. Mayer M, Meyer B (1999) Angew Chem Int Ed 38:1784–1788
30. Morris GM, Huey R, Lindstrom W, Sanner MF, Belew RK, Goodsell DS, Olson AJ (2009) J Comput Chem 30:2785–2791
31. Vreven T, Morokuma K, Farkas O, Schlegel HB, Frisch MJ (2003) J Comput Chem 24:760–769
32. Harris WR, Pecoraro VL (1983) Biochemistry 22:292–299
33. James NG, Berger CL, Byrne SL, Smith VC, MacGillivray RT, Mason AB (2007) Biochemistry 46:10603–10611
34. Sun H, Cox MC, Li H, Sadler PJ (1997) Struct Bond 88:71–102
35. Harris WR, Messori L (2002) Coord Chem Rev 228:237–262
36. Farkas E, Kozma E, Kiss T, Toth I, Kurzak B (1995) J Chem Soc Dalton Trans 447–481
37. Chasteen ND, Grady JK, Holloway CE (1986) Inorg Chem 25:2754–2760
38. Lakowicz JR (2006) Principles of fluorescence spectroscopy, 3rd edn. Springer, New York
39. Zékány L, Nagypál I (1985) In: Leggett DL (ed) Computational methods for the determination of stability constants. Plenum, New York, pp 291–353
40. Allen FH (2002) Acta Crystallogr B 58:380–388
41. Wang Y, Zhang WX, Li YQ, Ye L, Yang GD (1999) Chem Mater 11:530–532
42. Frisch MJ, Trucks GW, Schlegel HB, Scuseria GE, Robb MA, Cheeseman JR, Scalmani G, Barone V, Mennucci B, Petersson GA, Nakatsuji H, Caricato M, Li X, Hratchian HP, Izmaylov AF, Bloino J, Zheng G, Sonnenberg JL, Hada M, Ehara M, Toyota K, Fukuda R, Hasegawa J, Ishida M, Nakajima T, Honda Y, Kitao O, Nakai H, Vreven T, Montgomery JAJ, Peralta JE, Ogliaro F, Bearpark M, Heyd JJ, Brothers E, Kudin KN, Staroverov VN, Kobayashi R, Normand J, Raghavachari K, Rendell A, Burant JC, Iyengar SS, Tomasi J, Cossi M, Rega N, Millam NJ, Klene M, Knox JE, Cross JB, Bakken V, Adamo C, Jaramillo J, Gomperts R, Stratmann RE, Yazyev O, Austin AJ, Cammi R, Pomelli C, Ochterski JW, Martin RL, Morokuma K, Zakrzewski VG, Voth GA, Salvador P, Dannenberg JJ, Dapprich S, Daniels AD, Farkas Ö, Foresman JB, Ortiz JV, Cioslowski J, Fox DJ (2009) Gaussian 09, revision D.01. Gaussian, Wallingford
43. Becke AD (1988) Phys Rev A 38:3098–3100
44. Miehlich B, Savin A, Stoll H, Preuss H (1989) Chem Phys Lett 157:200–206
45. Berman HM, Westbrook J, Feng Z, Gilliland G, Bhat TN, Weissig H, Shindyalov IN, Bourne PE (2000) Nucleic Acids Res 28:235–242
46. Ghuman J, Zunszain PA, Petitpas I, Bhattacharya AA, Otagiri M, Curry S (2005) J Mol Biol 353:38–52
47. Wang ZM, Ho JX, Ruble JR, Rose J, Ruker F, Ellenburg M, Murphy R, Click J, Soistman E, Wilkerson L, Carter DC (2013) Biochim Biophys Acta 1830:5356–5374
48. Pettersen EF, Goddard TD, Huang CC, Couch GS, Greenblatt DM, Meng EC, Ferrin TE (2004) J Comput Chem 25:1605–1612